The Effect of Grain Orientation on Fracture Morphology during the High Cycle Fatigue of Ti-6Al-4V

Ioannis Bantounas, David Dye, Trevor C Lindley

Department of Materials, Imperial College, South Kensington, London SW7 2AZ, UK

Abstract

Three different product forms of Ti-6Al-4V, uni-directionally (UD) and cross-rolled (XR) plate and forged bar, have been cyclically loaded within the high cycle fatigue (HCF) regime to investigate fatigue crack initiation. The fracture surfaces of fatigued specimens contained large regions of neighbouring facets. The majority of facets examined had a near-basal fracture plane. It was shown that grains favouring crack initiation were primarily those with misorientations between 15–40° from the loading direction whereas other orientations served as crack growth paths. This implies that the formation of a facet requires a combination of a moderately high Schmid (m) factor for basal slip coupled with a tensile component perpendicular to the basal plane. The large regions of neighbouring facets on the fracture surface were found to be a consequence of cracking within a macrozone unfavourably oriented for slip found within the microstructure, i.e., one with its c-axis near to the loading direction.

Key words: Titanium alloys, Fatigue, Texture, Electron backscattered diffraction (EBSD), Quantitative Tilt Fractography (QTF)

1. Introduction

Mechanical properties of titanium alloys are heavily dependent on processing history [1]. A general desired microstructural condition for aerospace components is the fine grained bi-modal microstructure, where refinement of the grain size is known to increase the yield stress, ductility and improve fatigue resistance [1, 2]. Recently focus has been diverted to the effects of texture and local grain variations on fatigue performance of such alloys. The general trend in fatigue-texture relations being that a degradation in fatigue life is observed when loading parallel to the c-axis of the hexagonal α phase in a textured titanium alloy [1, 3, 4].

Investigations of the fracture morphology of titanium alloys has shown that crack initiation is associated with faceting of unfavourably oriented grains. Such facets have been observed to form near the basal plane, implying that basal slip is a common cause of crack initiation under conditions of fatigue loading [5, 6]. A study by Ward-Close *et al.* [6] characterised the fracture features observed in an α titanium alloy and related them to their grain orientation, constructing a stereographic projection of grain orientation and fracture feature. The results of this work showed that grains oriented within 40° to 60° out of the plane of maximum tensile stress would crack via a facet mechanism, the angle being dependent on testing environment.

Under conditions of dwell fatigue, initiation sites are generally observed to occur in grains whose c-axis is near parallel to the loading direction [5, 7]. In such grains the basal slip system is not at its maximum critical resolved shear stress value, yet fractures are observed to be close to the basal pole. A model to account for this observation has been suggested in the work of Bache and Evans [8], based on the Stroh pile-up model [9], and later developed by Dunne *et al.* [10]. A similar model to explain load partitioning under creep and dwell fatigue conditions has also been developed by Mills and co-workers [11, 12]; both models illustrate the effect of load partitioning from a soft grain onto a neighbouring hard grain and possible critical grain combinations for crack initiation have been suggested.

The current study examines the effects of grain orientation on fracture morphology. More particularly it is an attempt to elucidate the role of grain orientation on the fractographic features observed. In the present study facets have been observed to form on grains oriented with their c-axis between 0° and 90° from the loading direction (LD). Observation of neighbouring grains, comparisons between isolated facets and subsurface and secondary cracks have been made in an effort to distinguish the orientations responsible for crack initiation and those that assist crack growth.

2. Experimental

The Ti-6Al-4V material examined was provided by Rolls-Royce Plc, Derby in three product forms, uni-directionally (UD) and cross-rolled (XR) plate and forged bar. The microstructure of the plate material consisted of equiaxed

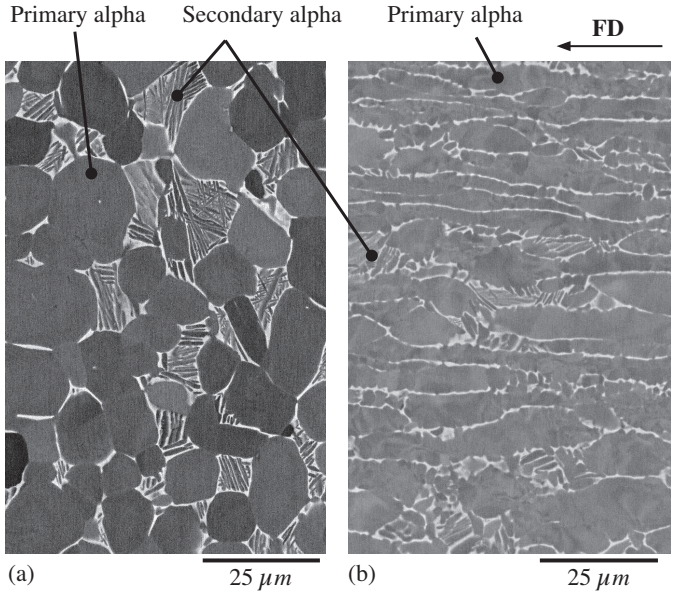

Figure 1: Backscattered electron images showing the microstructure of (a) the plate and (b) forged bar product forms.

(also termed globular) primary alpha (α_p) grains in a transformed beta (β) matrix consisting of secondary alpha (α_s) laths separated by a thin layer of β phase, Figure 1(a). The area fraction of α_p was $\approx 80\%$ in both plate product forms with the XR and UD materials having an α_p grain size of 12.3 µm±1.3 µm and 14.2 µm±2.0 µm respectively. The microstructure of the bar product form had elongated α_p grains that stretch along the forging direction (FD) separated by β at the grain boundaries, Figure 1(b). The area fraction of α_p was $\approx 76\%$ with the grains having a width of 5.9 µm±0.3 µm and an aspect ratio of $\sim$ 1:6.

Fatigue tests were performed using an Amsler Vibrophore HFP20 machine under displacement control at a stress ratio (R) of 0.3 in the high cycle fatigue (HCF) regime using the step-test method [13]. The loading direction was set parallel to the rolling and forging directions of the plate and bar product forms, respectively. Samples were consequently sectioned perpendicular to the fracture plane in order to expose the underlying microstructure of the fractured grains. Crystal orientation maps (COMs) have been obtained from the fracture cross-section in order to relate fracture features to the orientation of the underlying grains. The use of quantitative tilt fractography (QTF) allows determination of the spatial orientation of planar fracture features, such as faceted and striated grains. A combination of the COM and QTF data can provide information on the crystal plane responsible for fracture. The QTF technique used in the present study follows closely that outlined by Slavik *et al.* [14].

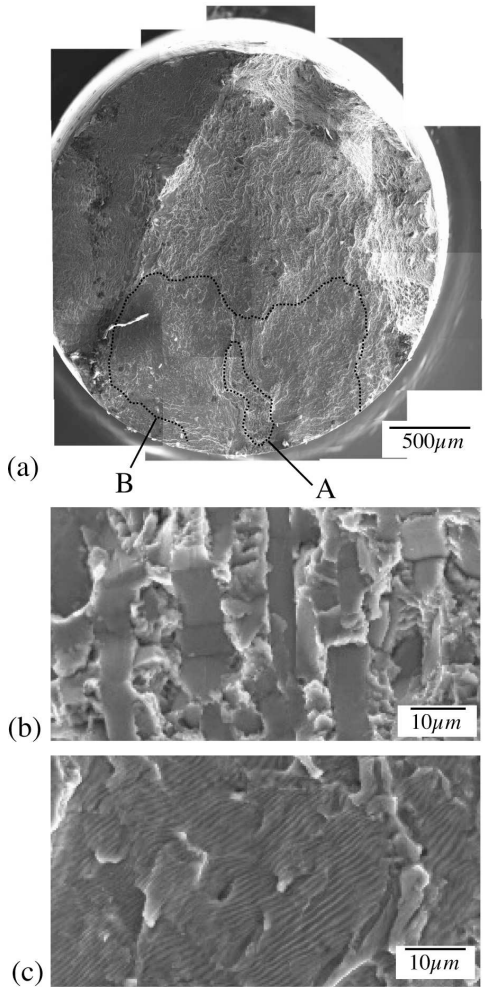

Figure 2: Secondary electron images showing (a) a fracture surface with highlighted faceted region A and striated region B, (b) an example of facets from region A and (c) striations from region B.

3. Results

Typically observed fracture surfaces of the three product forms during this study revealed the presence of large areas of continuous faceted grains, Figures 2(a) and (b). These large regions usually comprise of hundreds of neighbouring faceted grains. As such it is important to know which of these grains are responsible for crack initiation and which accommodate crack growth. Regions further away from the faceted initiation sites have been observed to accommodate crack advance by the formation of ductile striations, Figures 2(a) and (c).

3.1. Orientation of faceted grains

During fatigue loading, grains of different orientations will deform via different slip mechanisms depending on which slip system was most favourable. Activation of slip in single crystals is dependent on two factors: 1) the Schmid factor (m), which is a function of grain orientation relative to the loading direction (LD), and 2) the critical resolved shear stress (CRSS) required to activate the

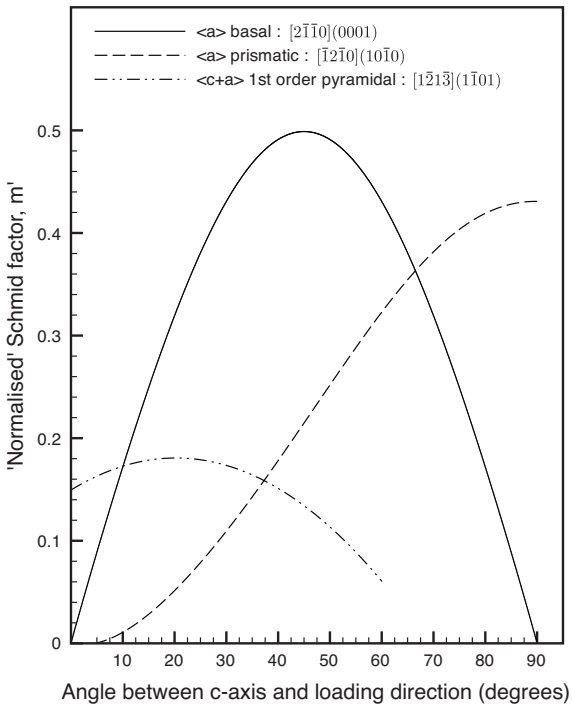

Figure 3: Graph of 'normalised' Schmid factor versus the angle between the c-axis and the loading direction for basal and prismatic $<a>$ slip and 1^{st} order pyramidal $<c+a>$ slip.

slip system. Polycrystalline materials are more complex in that there can be load distribution between neighbouring grains influencing slip activity [10, 11, 12].

In an attempt to model the active slip system as a function of misorientation between the LD and the c-axis of a given grain (γ_{LD}) a plot of 'normalised' Schmid factor (m') versus γ_{LD} has been plotted, Figure 3. The equation for m' is given by

$$m' = m \cdot (\tau_{min}/\tau_{<uvtw>\{hkil\}}) \quad (1)$$

where $\tau_{min}/\tau_{<uvtw>\{hkil\}}$ is the ratio of the CRSS of a given slip system ($\tau_{<uvtw>\{hkil\}}$) to the CRSS of the easiest activated slip system (τ_{min}), in this case basal or prismatic $<a>$ slip [3]. Ratios for the CRSS values used for $<a>$ basal, $<a>$ prismatic and $<c+a>$ pyramidal slip are $1:1:2.64$, similar to those used in Refs [10, 15].

From the graph in Figure 3 it can be seen that when γ_{LD} is within 0° and 10° $<c+a>_{pyr}$ slip will be dominant. An increase in the misorientation angle between 10° and 66.7° will see the principal slip system being $<a>_{basal}$. A further increase in c-axis misorientation from 66.7° to 90° orients the grain for $<a>_{prism}$ slip. In essence this graph provides two boundaries, one at 10° for the transition between $<c+a>_{pyr}$ and $<a>_{basal}$ slip and one at 66.7° for the transition between $<a>_{basal}$ and $<a>_{prism}$ slip.

Possessing an indication of the active slip mode as a function of c-axis misorientation from the LD, we can now examine the c-axis misorientation for faceted grains and relate cracking to the active slip system. The histogram

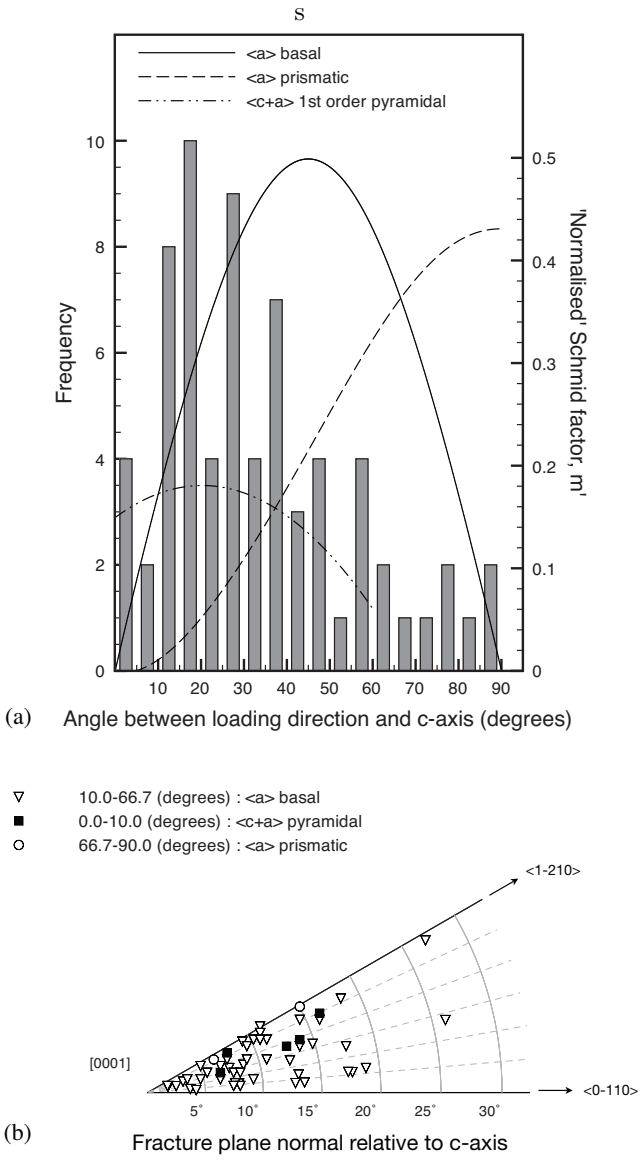

(a)

(b)

Figure 4: (a) Histogram of γ_{LD} against frequency of faceted grains grouped into 5° bins, overlaid with γ_{LD} against 'normalised' Schmid factor. (b) An inverse pole figure (IPF) showing the orientation of the facet plane normal relative to the c-axis of each fractured grain. The fracture planes have been grouped according their c-axis misorientations relative to the LD (0.0–10.0°, 10.0–66.7° and 66.7–90.0°).

in Figure 4(a) shows the c-axis misorientation of faceted grains against the number of faceted grains grouped into 5° bins. A total of 69 grains were analysed. The orientation of the facet planes relative to the c-axis of these grains, for 58 of the 69 grains, is depicted in Figure 4(b).

The peculiar finding when comparing Figure 4(a) and (b) is that even though faceted fractures are found in grains oriented between 0 °and 90 °, the majority of the fracture planes are 'near' basal. This means that grains which are oriented for prismatic $<a>$ or pyramidal $<c+a>$ slip will fracture near the basal plane. In order to rationalise these observations each slip system will now be dis-

cussed in turn.

Facets oriented for <c + a> slip

Grains favouring <c + a> pyramidal slip have c-axis misorientations between 0° and 10.0° from the LD, Figure 4(a). These grains have been found to crack near the basal plane, closed squares in Figure 4(b), and not along the pyramidal plane for which they are favourably oriented for slip. Speculation previously has suggested that such grains act as crack initiation sites under conditions of load redistribution and are a more common aspect of dwell-fatigue loading [5, 7]. In such cases, grains with a c-axis misorientation within 10° of the LD, referred to as 'hard' grains, neighbour grains with a c-axis orientation near perpendicular to the LD, 'soft' grains [10, 12]. The soft grain is thought to deform first, leading to a pile-up of dislocations at the boundary of the hard grain. This dislocation pile-up introduces a shear component on the hard grain, which in conjunction with a tensile component near-parallel to the c-axis will lead to cracking along the basal plane, after the Stroh pile-up model [9]. Stresses accumulated at the boundary of the soft and hard grains are more pronounced under stress-controlled testing.

Examination of the grains surrounding the 5 faceted grains oriented for <c + a> slip showed that none of their neighbours were oriented such that their c-axis was perpendicular to the loading direction. Three cases were found where the neighbouring grains were oriented for basal slip. These basal oriented grains had either formed near-basal facets or secondary cracks along the basal trace. The possibility of basal slip oriented grains playing the role of the 'soft' grains in the load shedding model can not be ruled out; since loading was displacement-controlled under non-dwell fatigue conditions it is unlikely that grains oriented for <c + a> slip were grains where cracking first initiated. A more probable scenario is that these grains cracked along the basal plane due to increased stresses at the crack tip within a neighbouring basal oriented grain which fractured due to a slip mechanism.

Facets oriented for basal <a> slip

Grains with c-axis misorientations that lie within 10.0° to 66.7° are oriented for basal slip, Figure 4(a). The orientation of the facet plane relative to the c-axis for 48 of the 58 basal <a> grains is shown as inverted open triangles in Figure 4(b). The majority of these grains have fractured within 15 °of the c-axis with maximum deviations approaching misorientations of 27 °. The general observation that grains oriented for basal slip will fracture near the basal plane implies that accumulation of basal dislocations are accountable for crack initiation in these grains.

Facets oriented for prismatic <a> slip

A total of 7 of the 69 grains analysed were oriented for prismatic slip and formed a faceted fracture, see misorientations between $66.7 < \gamma_{LD} \leq 90°$ in Figure 4(a). Data has been obtained for the fracture plane of 2 of the

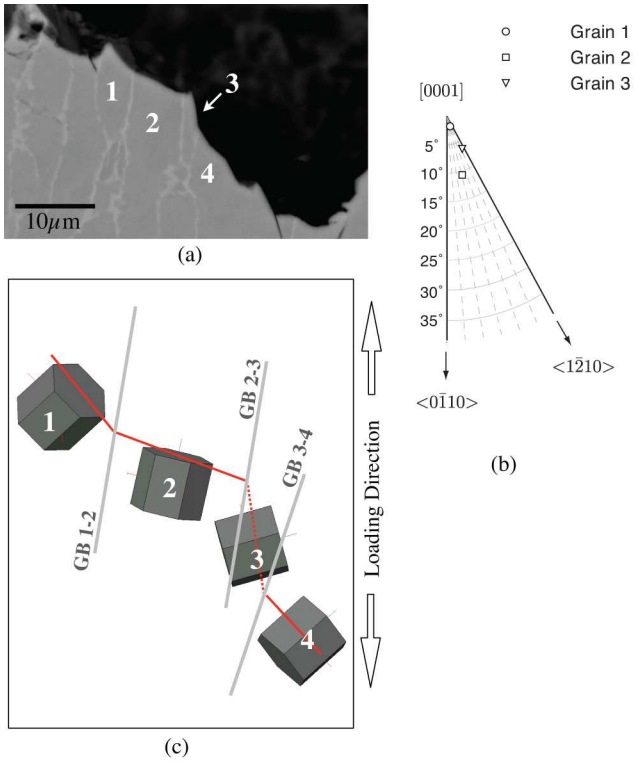

Figure 5: (a) Backscattered electron image of the fracture surface cross-section showing grains 1–4, (b) orientation of fracture plane relative to the c-axis for grains 1–3 and (c) schematic illustration of grain orientations and fracture paths for grains 1–4, solid fracture paths are assumed to have formed prior to the dashed one.

7 grains, open circles in Figure 4(b). Fracture of these planes are both 'near' basal and can not be accounted for by slip on the prismatic plane; an alternative explanation for faceting of these grains must therefore be provided.

An example of the grains surrounding a grain that is oriented for prismatic slip and has a near basal fracture plane is considered. The cross-section of 4 fractured grains labelled 1–4 are shown in Figure 5(a). Grains 1, 2 and 4 are favourably oriented for basal slip and grain 3 is oriented for prismatic <a> slip. All 4 grains have fractured near the basal plane, Figure 5(b). Assuming that all grains had active slip systems prior to cracking and knowing that grains 1, 2 and 4 fractured along the plane for which they were favourably oriented, whereas grain 3 did not, it may be presumed that grains 1, 2 and 4 fractured prior to grain 3. In such a case grain 3 will act as a non-cracked ligament between grains 2 and 4, Figure 5(c). Grain 3 could hence provide a link between grains 2 and 4 if cracking along the basal plane is accommodated. Finally, grain 3 is believed to have fractured along a plane for which slip is unlikely as a means of assisting an 'easy' fracture path between grains 2 and 4.

Evidence of such continuous faceting with large misorientations can be seen in Figure 6(a). The misorientation between planes A and B is 41° and that between plane B and C is 31°. Therefore a fracture facet that appears

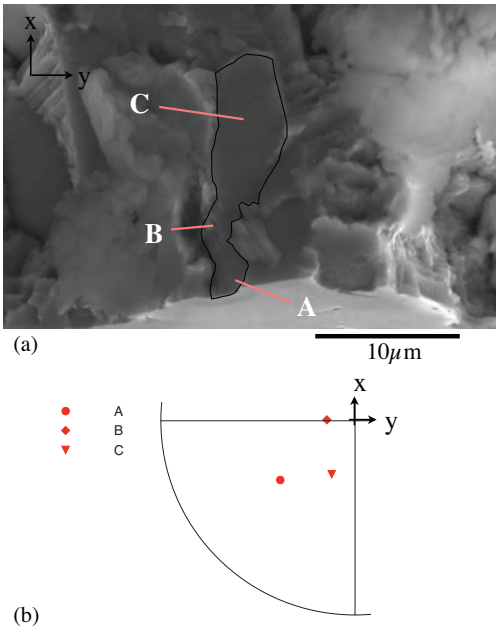

Figure 6: (a) Secondary electron image from a faceted region exhibiting a 'continuous' facet that contains three different fracture planes (A, B and C), obtained at a tilt angle of 20°, and (b) a quadrant of a pole figure depicting the orientation of the three facet planes relative to the loading direction, z-axis.

to be one continuous grain had within it three distinct orientations, Figure 6(b).

Thus, continuous facets can form across grains with large misorientations. In addition, cracking of 'irregular' planes in grains oriented for slip in slip systems that do not incorporate the fracture plane are believed to be influenced by prior cracking in neighbouring grains and are a consequence of accommodating crack propagation.

Isolated facets

In the context of this paper, an isolated facet is defined as a faceted grain whose neighbours have not fractured via facet formation. The concept behind examining isolated facets is to obtain the orientations of grains that are possible initiation sites, in that these grains did not fracture as a means of accommodating crack growth but rather due to slip. All isolated facets examined fractured near the plane for which slip was most likely.

In order to confirm that these facets were indeed isolated, the cross-sectioned region of the fracture surface had to be mapped onto a series of high magnification images obtained from the fracture surface prior to sectioning, Figure 7(a) and (b). In this way, all grains surrounding the facetted grain in question could be examined and the grain could be classified as isolated or non-isolated with confidence.

The filtering procedure is shown in Figure 8 where an example of a non-isolated and an isolated facet, A and B respectively, are depicted. Facet A in Figure 8(a) has 7 neighbouring grains, labelled 1–7. Of these 7 grains, 5

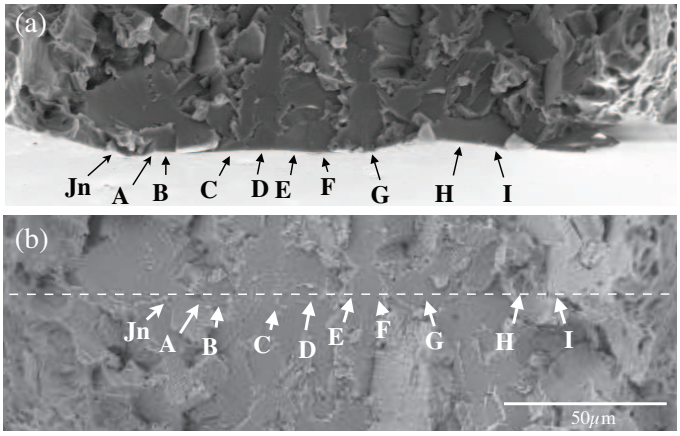

Figure 7: Secondary electron image of (a) cross-section of a fracture surface obtained at a 20° tilt angle, and (b) same location prior to sectioning showing complete area of 10 faceted grains labelled A – J_n, sample sectioned along dashed line.

cracked by faceting (grains 1, 2, 4, 5 and 6). For the case of Facet B, Figure 8(b), all 5 neighbouring grains have not fractured via facet formation. Grain B is hence an example of an isolated facet whereas grain A is an example of a non-isolated facet.

From the whole data set, 5 grains were classified as isolated facets, all of which were oriented for basal <a> slip, Figure 9(a), and also fractured near the basal plane, Figure 9(b). This observation shows that since these grains are not a consequence of neighbouring grains influencing a crack path upon them, they are probable initiation sites.

3.2. Secondary and subsurface cracking

Secondary and subsurface cracks have been located from the fracture surface cross-sections examined. Cracking within single grains were distinguished from grain boundary (GB) cracks by comparing the backscattered electron images (BEIs) to the equivalent crystal orientation maps

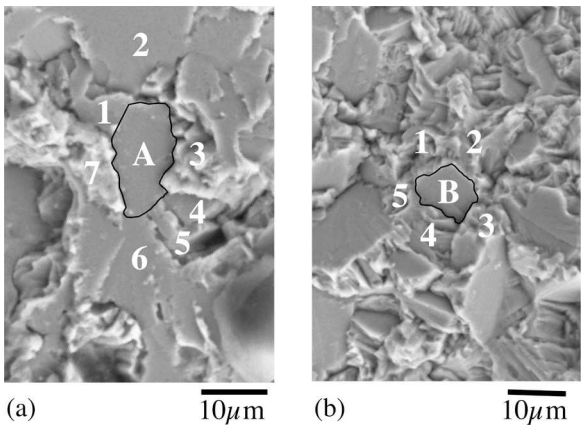

Figure 8: Secondary electron image of a fracture surface showing an example of (a) a non-isolated facet (A) neighbouring 7 grains, and (b) an isolated facet (B) neighbouring 5 non-faceted grains.

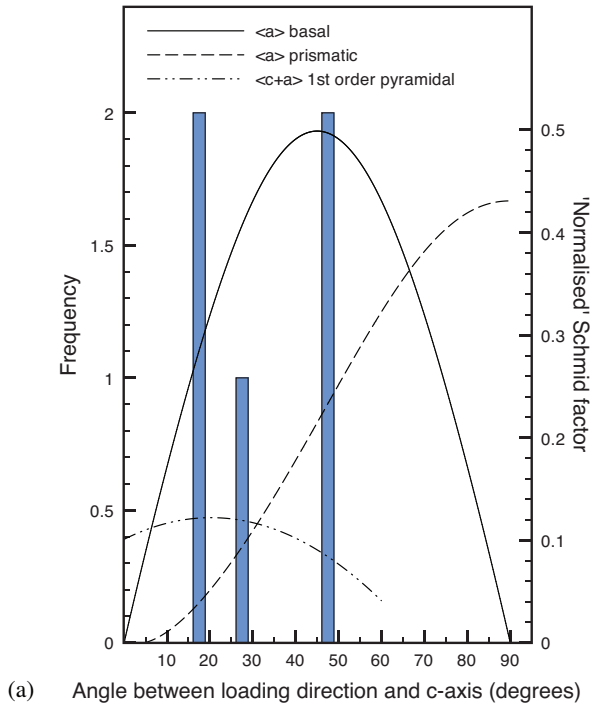

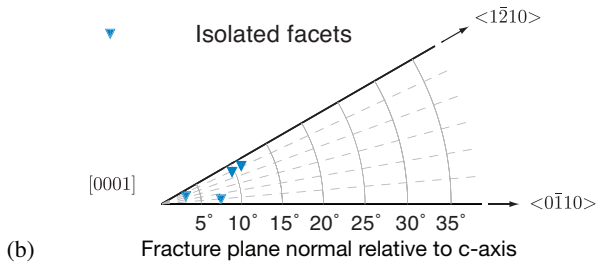

Figure 9: (a) Histogram of γ_{LD} against frequency for isolated facets grouped into 5° bins. The graph has been overlaid on a plot of γ_{LD} against 'normalised' Schmid factor, and (b) IPF showing the orientation of the facet plane normal relative to the c-axis for 4 of the 5 grains in (a).

(COMs) and assigning each grain to a particular orientation. The orientation of each grain was then plotted onto a pole figure along with the great circle of the plane believed to contain the crack, the trace of the plane onto the cross-sectioned plane (X1-Y1 plane) and finally the intersection of the crack with the X1-Y1 plane. The orientation of the projected crack was then compared to the projection of the plane and the fracture plane determined. An example of the procedure applied to a secondary crack that fractured along the basal trace is shown in Figure 10.

Orientations of grains containing both secondary and subsurface cracks were separated into basal and non-basal fractures and plotted onto a histogram of misorientation angle against frequency, Figure 11(a). From this graph it can be observed that even though the majority of basal fractures were contained within the orientations for basal slip, there were still basal fractures in grains oriented for prismatic slip as well as non-basal fractures within the

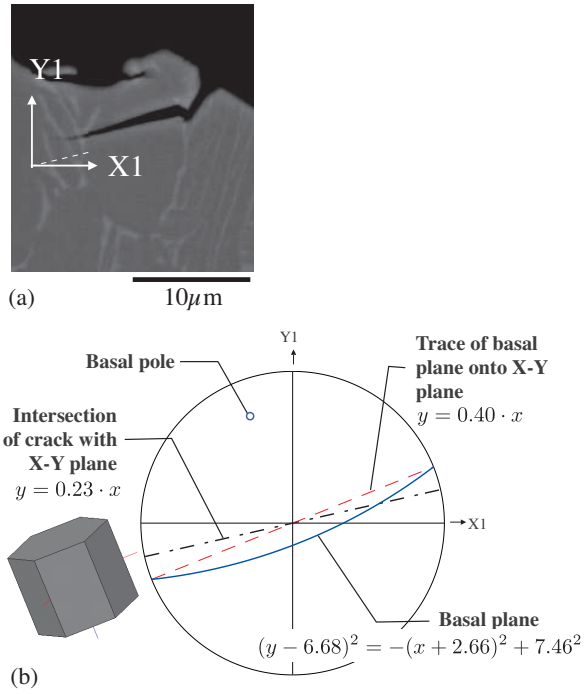

Figure 10: (a) BEI of a secondary crack in a primary α grain, and (b) pole figure showing the basal pole, basal plane and basal trace of the primary α grain along with the intersection of the crack onto the X1-Y1 plane. Equations defining each projection are included.

basal slip regime. A separation of this data shows that it is the grains that contain the secondary cracks which contribute to the fractures which do not obey the m' graph, Figure 11(b). When the data from the subsurface cracks is displayed independently, grains oriented for basal slip are observed to fracture along the basal trace whereas those oriented for prismatic slip show non-basal fractures, Figure 11(c). This supports the argument that grains that formed facets on 'irregular' planes did so as a means of accommodating cracking as opposed to being crack initiating grains.

Supposing that these subsurface cracks do not extend far into the cross-sectioned face, to the point where they intersect the fracture surface, and that they are generally contained within a maximum of 3 grains, such grains may be assumed to have initiated on their own accord due to accumulation of slip. Such a claim is fairly probable as the majority of subsurface cracks belong to grains which have also fractured. With this in mind it may be assumed that multiple slip bands form along a common plane within the same grain.

Secondary cracks are extensions of the fracture surface into the material. The fact that they do not always crack along their presumed slip plane, whereas the subsurface cracks do, agrees with the suggestions for 'irregular' fracture planes in the previous section. In that 'irregular' fracture planes are a consequence of crack growth, whereas subsurface and 'isolated' facets form due to slip along the slip system for which they are favourably ori-

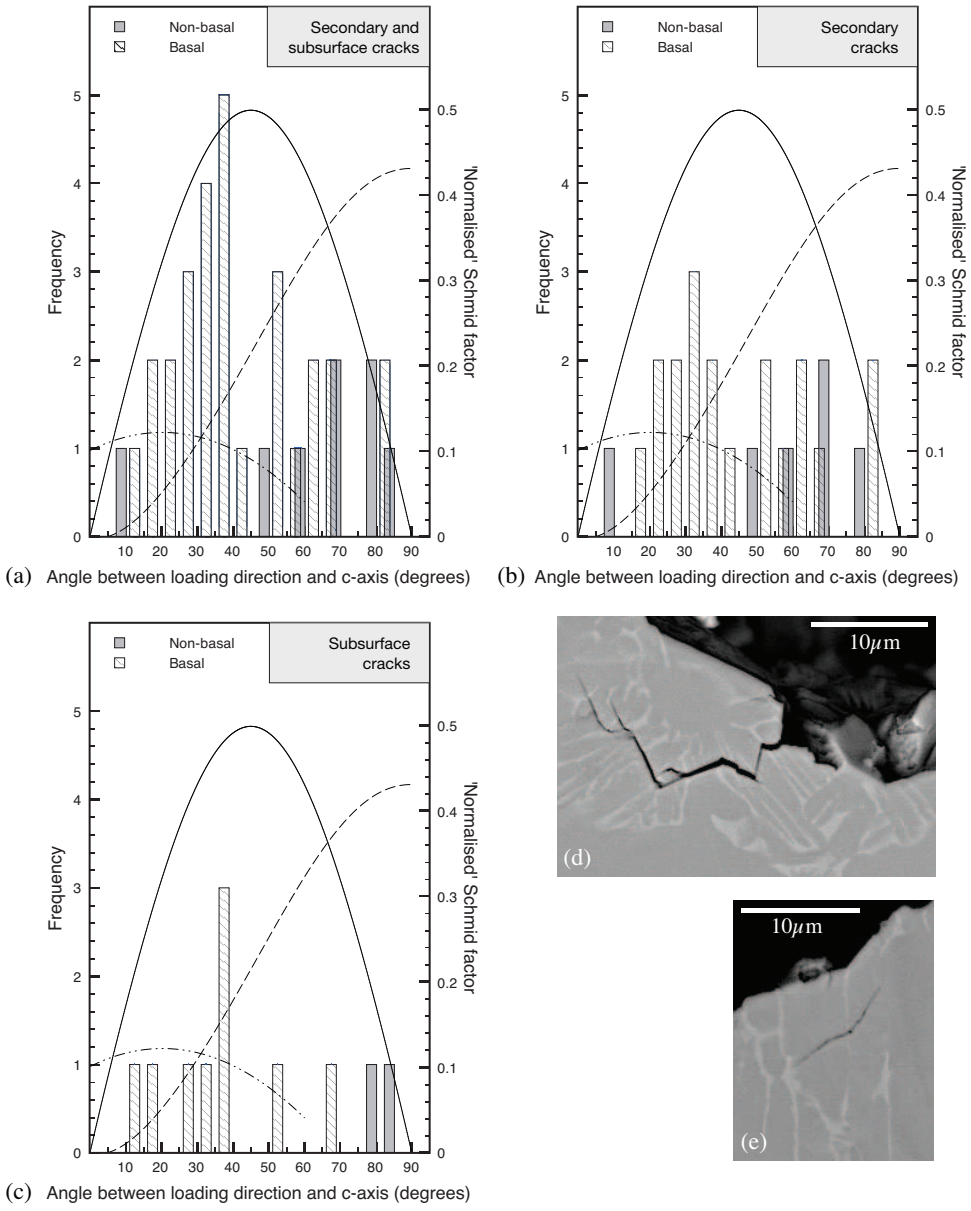

Figure 11: Histogram of c-axis misorientation against frequency for data containing (a) both secondary and subsurface cracked grains, (b) grains with secondary cracks and (c) grains with subsurface cracks. Images (d) and (e) are BEIs showing examples of secondary and subsurface cracking respectively.

ented. Later on, in the discussion, a method is suggested to filter through the data obtained and suggest grain orientations that are more likely to initiate a crack than others.

3.3. Striated grains

The histogram in Figure 12(a) shows the misorientation angle vs frequency for grains that exhibited striated crack growth. It can be seen that the majority of such grains lie in the prismatic slip regime with a few lying on either side of the $<a>$ basal to $<c+a>$ pyramidal boundary. The absence of striated grains within the basal slip regime supports the requirement for symmetric slip about the crack tip for the ductile formation of striations. This condition cannot be satisfied by basal slip as basal planes, within an individual grain, lie parallel to one another. Grains oriented for prismatic slip exhibit fracture planes away from the basal plane and closer to the $\{0\bar{1}10\}$ and $\{1\bar{2}10\}$ planes, open circles in Figure 12(b). However, grains close to the $<c+a>$ slip regime fracture near the basal plane, open inverted triangles in Figure 12(b).

Striations oriented for prismatic slip that have fractured close to either the $\{0\bar{1}10\}$ or $\{1\bar{2}10\}$ plane can be accounted for by the activation of symmetric prismatic slip planes about the fracture plane. Activation of the $[\bar{1}\bar{1}20](\bar{1}100)$ and $[\bar{1}2\bar{1}0](10\bar{1}0)$ slip systems symmetrically about the $(01\bar{1}0)$ plane will produce striations lying along

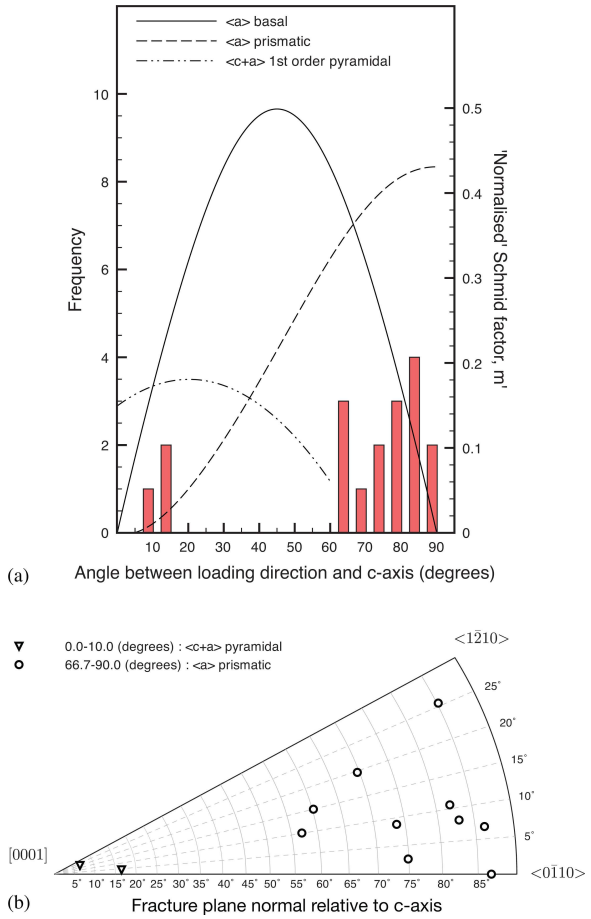

Figure 12: (a) Histogram of c-axis misorientation against frequency of occurrence of grains exhibiting a striated fracture morphology (b) orientation of fracture plane normal relative to the c-axis for the striated grains shown in (a). Inverted open triangles are fractured grains with c-axis misorientations close to the $<c+a>$ slip regime and open circles are those close to $<a>$ prismatic slip.

the [0001] direction and account for striated fracture planes lying on $\{0\bar{1}10\}$ planes [16], see example of grain A in Figure 13(a) and table 1. Grains that fractured on $\{1\bar{2}10\}$ are loaded parallel to a $\{10\bar{1}0\}$ plane and activate both the $[2\bar{1}\bar{1}0](01\bar{1}0)$ and $[1\bar{2}10](10\bar{1}0)$ slip systems, see grain B in Figure 13(b) and Table 1. Striated grains with fracture planes near the basal plane are a result of symmetric activation of symmetric $<11\bar{2}3>$ slip systems about the crack tip [17], Figure 13(c).

There were a few striated grains that lie on the basal

Table 1: Schmid factors for basal and prismatic $<a>$ slip for grains A and B that exhibited a striated fracture morphology.

		Schmid factor	
Plane	Slip system	Grain A	Grain B
Prismatic	$(a/3)[2\bar{1}\bar{1}0](01\bar{1}0)$	0.08	0.42
	$(a/3)[\bar{1}2\bar{1}0](10\bar{1}0)$	0.46	0.44
	$(a/3)[\bar{1}\bar{1}20](\bar{1}100)$	0.38	0.01

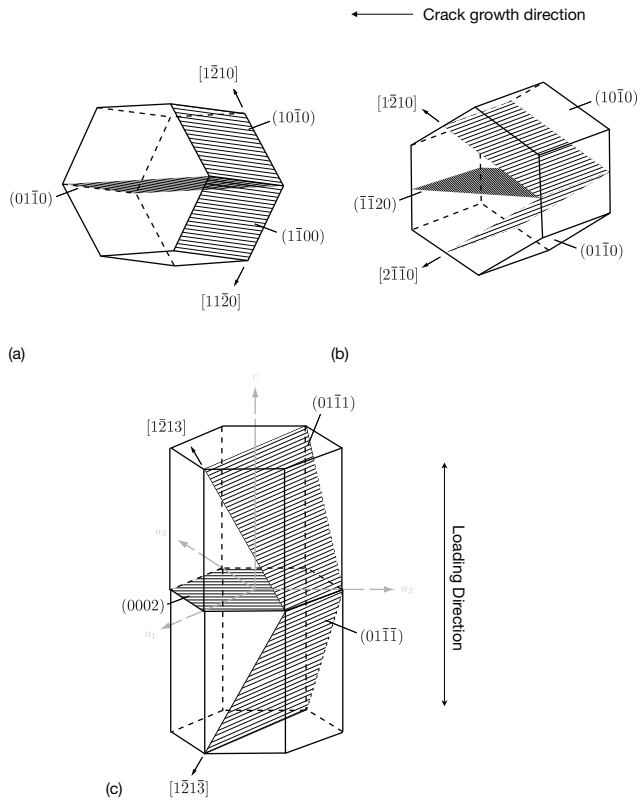

Figure 13: Illustration of hexagonal prisms depicting the activated slip systems for striated grains with nominal fractures on the (a) $(01\bar{1}0)$, (b) $(\bar{1}\bar{1}20)$ and (c) (0002) planes.

slip side of the boundaries between basal and $<c+a>$ slip as well as basal and prismatic slip. The occurrence of these grains are believed to be due to the tri-axial stress state at the crack front of a propagating crack. This will change the loading conditions ahead of the crack tip and as such grains will not strictly obey the Schmid factor as calculated under uni-axial loading conditions.

4. Discussion

4.1. Grains favouring high cycle fatigue cracking

Examination of the fracture surface features observed after high cycle fatigue loading at a stress ratio, R, of 0.3 under displacement control shows that crack initiation in all three product forms is associated with large regions of faceted crack growth. The orientation and fracture plane of 58 grains exhibiting a facet morphology have been analysed. Results show that facets form in grains oriented within 0.0–90° of the principal loading direction, with the majority of facet planes having formed near the basal plane, Figure 4(a) and (b). A series of steps have been employed to distinguish between grains that are accountable for crack initiation and those that assist crack growth.

It has been shown that grains oriented for prismatic $<a>$ slip will fracture on 'irregular' planes as a means

of accommodating crack growth between grains oriented for basal slip. Prismatic oriented grains have been observed to crack along prismatic planes in subsurface cracks in this study, though no facets examined fractured near the prismatic plane. Grains oriented for prismatic $<a>$ slip have been reported to act as initiation sites in other studies [18, 19]. They are usually associated with crack initiation along a favourable prismatic plane, found to not grow as fast and contribute to a successfully propagating initiation site as do cracks in basal oriented grains, and are seen to act as initiation sites in regions where basal oriented grains are scarce.

Pyramidal $<c+a>$ slip oriented grains have not been found to obey the load shedding criteria, 'soft' grain neighbouring a 'hard' grain [10, 15]. In addition such failures are commonly the case under dwell-fatigue strain-controlled loading [20, 21], which was not the type of loading employed in this study. Prismatic $<a>$ and pyramidal $<c+a>$ oriented grains that cracked with a near basal facet morphology are believed to have done so as a means of assisting crack advance.

The elimination of $<c+a>$ pyramidal and prismatic $<a>$ slip oriented grains from possible initiation sites leaves the basal $<a>$ orientations liable for HCF failures. Since basal $<a>$ slip occupies 67% of the possible c-axis misorientations with the LD, it would be advantageous if an account of grains with a higher probability for cracking could be provided.

Looking at the histogram in Figure 4(a) it can be observed that the most frequently recorded facet orientations are when the c-axis misorientation is between 10° and 30° from the principal loading direction. At first this may appear to be the most likely orientation for facet formation, though one has to also consider the texture of the material. The histogram in Figure 14 shows the same data normalised by the basal texture obtained from an analysis of XRD pole figure data.

Normalising the data, as an attempt to remove texture effects, sees a similar trend for basal plane faceting with a small shift towards higher angles. Facets favour grains with c-axis misorientations within 15° to 40° from the loading direction. This has also been reported in the work of Bridier et. al [18] who observed basal cracking in grains oriented such that their Schmid factor for basal slip was greater than 0.2 and had a c-axis misorientation within 40° of the loading direction. As with the current work, it is curious that faceted grains are not more abundant within grains favouring basal slip, i.e., at angles close to 45° where $m \approx 0.5$. Grains oriented for cracking under HCF conditions tend to favour a combination of a moderately high Schmid factor coupled with a tensile stress component acting perpendicular to the basal plane [18].

4.2. Fatigue performance and texture

The data presented above shows that grains oriented with their c-axis at angles within the range of $10.0 - 66.7\,^{\circ}$ from the principal loading axis, i.e., grains oriented for basal $<a>$ slip, are grains which contain facets and act as fatigue cracking initiation sites. This orientation range comprises 63% of the possible c-axis misorientations, the remaining 11.1% belongs to the pyramidal $<c+a>$ regime and 25.9% to $<a>$ prismatic slip. With this in mind it is important to note that there is a small range of orientations for which basal faceting is not favourable.

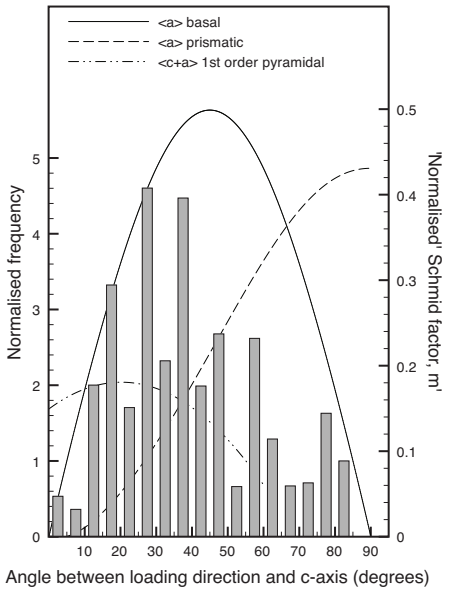

Figure 14: Histogram of c-axis misorientation against frequency for faceted grains normalised against basal pole intensities.

The three pole figures in Figure 15 represent the {0002} texture of the three Ti-6Al-4V product forms tested. Loading directions are out of the page and the dashed lines designate the transition between $<c+a>$ pyramidal, $<a>$ basal and $<a>$ prismatic slip. One can note that the bar product form contains the smallest number of grains within the $<a>$ basal slip regime, followed by the UD and finally the XR samples. The same trend is observed when one examines the intensities of basal grains within the basal cracking regime, encompassing the shaded region. The fatigue performance of the three materials also follow the same pattern. Longest fatigue lives are observed by the bar material followed by the UD with the XR product form exhibiting the poorest performance of the three, Figure 16.

The number of grains favourably oriented for facet formation hence play a role in determining the fatigue performance of the alloy. This has been well documented in other studies where fatigue performance has been shown to improve when loading perpendicular to the c-axis of heavily textured materials [1, 3, 4, 22, 23]. It is thus more favourable to activate the $<a>$ prismatic slip system. Even though subsurface cracks have been reported to initiate along prismatic planes, they are generally reported to not evolve into propagating cracks [18].

4.3. Microtexture and crack initiation sites

A crystal orientation map (COM) obtained from the UD product form is shown in Figure 17(a). Grains have been coloured according the inverse pole figure (IPF) shown above the COM, colouring is relative to the TD. Three areas have been labelled corresponding to regions of commonly oriented neighbouring grains. Macrozones I and II consist of densely clustered grains with a common c-axis near parallel to the TD, whereas macrozone III has small clusters of commonly oriented grains.

The extent of these microtextured regions can be observed in Figure 17(b). Here the COM from Figure 17(a) has been mapped onto the polarised light microscopy image. The faint contrast observed is found to be linked to the clusters of commonly oriented grains, i.e., macrozones I and II. Microtextured regions have previously been observed using polarised light in the work of Le Biavant et. al [24] and have been termed 'ghost' structures, owing to their faint contrast. The dimensions of these macrotextured regions greatly exceed the grain size with macrozones being up to 100μm in thickness and stretching several millimetres along the RD.

In the COM displayed in Figure 18(a), which shows the same map as Figure 17(a), grains oriented for basal cracking (between 15° and 40° from the principal loading direction) have been coloured in white. The TD has been designated as the principal loading direction (LD). The map shows that macrozone III has the highest density of grains oriented for basal cracking, clustered in groups of 3 to 5 grains.

Misorientations within 15° of the LD have been coloured in red in Figure 18(b). A different view of the map can now

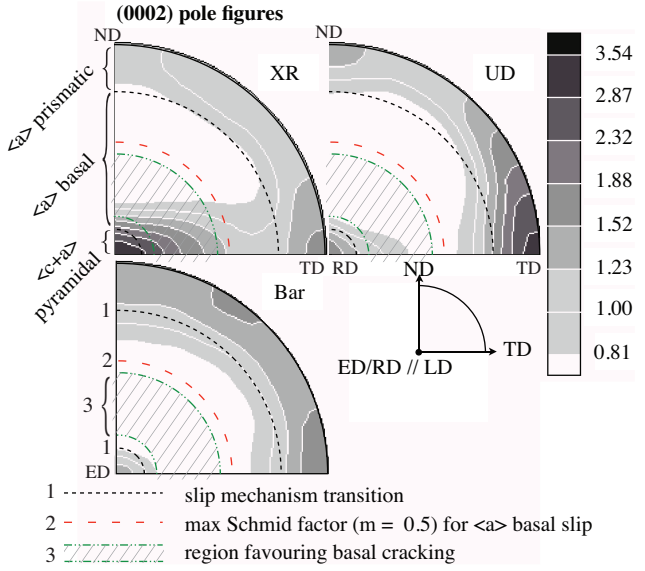

Figure 15: Basal (0002) pole figures of the three product forms (XR, UD and Bar) relative to the loading direction (LD). Overlaid, boundaries between the three slip systems (<a> basal, <a> prismatic and <$c+a$> pyramidal), the line of maximum Schmid factor for basal slip and shaded, the region within which basal cracking is favourable.

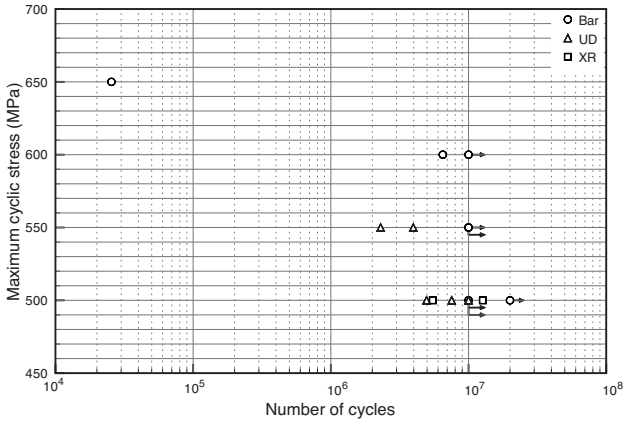

Figure 16: HCF data for the cross-rolled (XR), uni-directionally rolled (UD) and forged bar (Bar) product forms collected from the samples used for microscopy. Tests were conducted under displacement control with a stress ratio of 0.3.

be seen, the less densely occupied basal cracking grains in

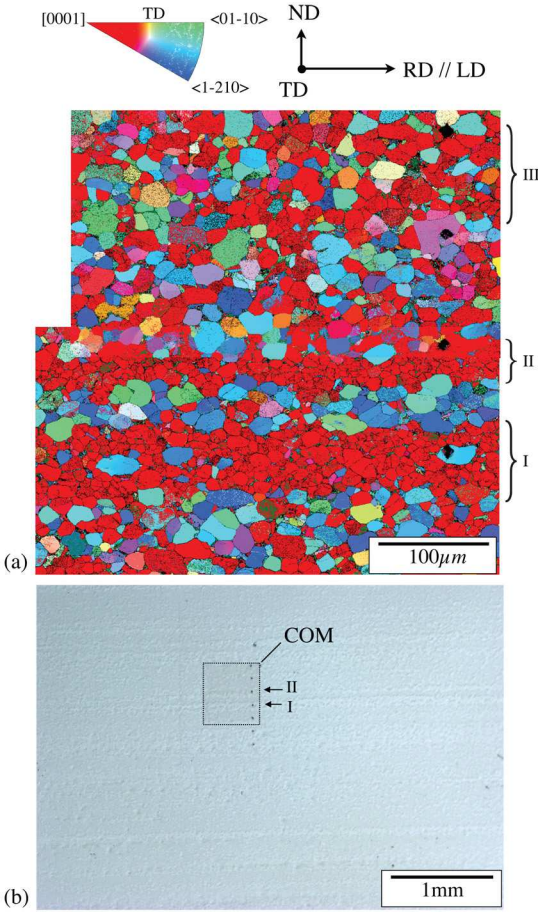

Figure 17: (a) COM from an area of the UD product form depicting microtextured regions I, II and III, and (b) low magnification optical micrograph faintly showing 'ghost' structure revealing the length-scale of the microtextured regions. The rectangle is the area from which the COM in (a) has been obtained.

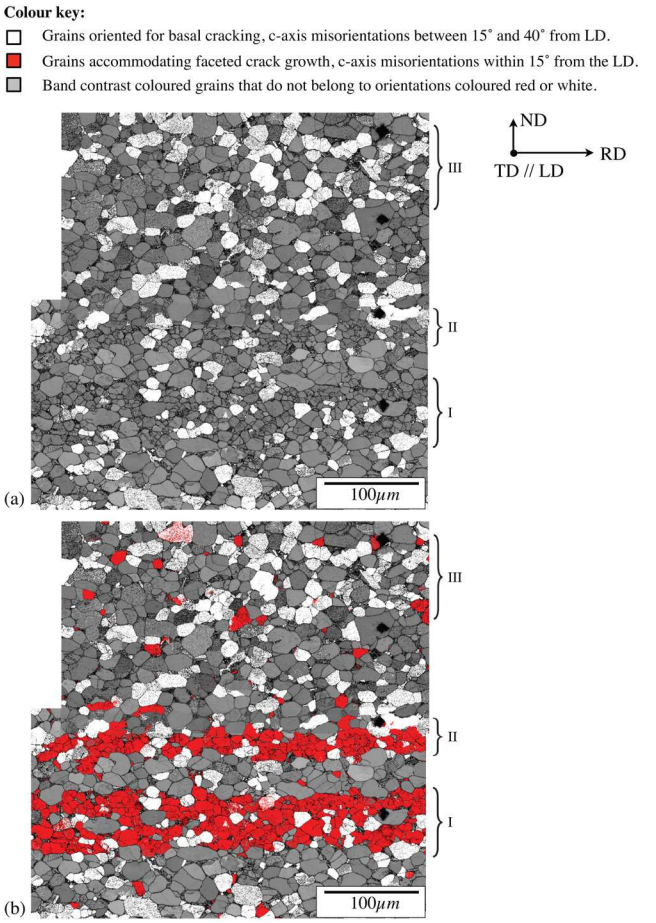

Figure 18: COM from an area of the UD product form, grains are coloured according to their pattern quality (band contrast) with (a) grains in white being favourably oriented for basal cracking, and (b) grains in red oriented within 15° of the LD (set parallel to the plate TD).

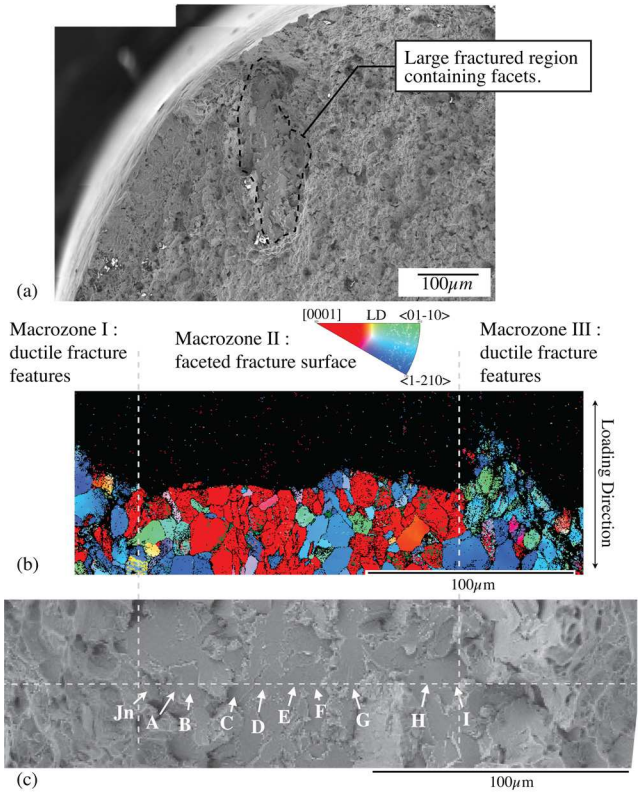

Figure 19: (a) Low magnification and (c) high magnification SEIs (Fig 7(b)) of the fracture surface from the XR material revealing a faceted region within an area of ductile fracture (obtained near the shear lip), (b) COM from the cross-section of the horizontal dashed line shown in (c) with grains coloured as shown in the IPF relative to the loading direction.

macrozones I and II are now seen to be linked by grains coloured in red. These grains have basal planes that are closer to being perpendicular to the LD than the basal cracking grains and are believed to be 'easy' cracking paths linking grains responsible for initiation [24] . The fact that these microtextured regions are found to stretch several millimetres across the material illustrates their role in faceted crack advance across large length scales.

Evidence of large areas containing neighbouring faceted grains is shown in Figure 19(a). The outlined region consists of faceted grains with the surrounding material having failed in a ductile manner. A section has been cut perpendicular to the fracture plane containing this region, Figure 19(b) and (c). The COM depicts three macrozones each corresponding to a change in fracture morphology. Macrozones I and III have c-axis misorientations near perpendicular to the LD and are responsible for the ductile fracture morphology that surrounds the faceted grains. The faceted region is seen to belong to grains in macrozone II which has its c-axis near parallel to the LD.

5. Conclusions

Fatigue samples from three product forms (forged bar, cross-rolled and uni-directionally rolled plate) of Ti-6Al-4V have been tested under uni-axial displacement controlled cyclic loading using a stress ratio of 0.3 with maximum stresses ranging between 500–650MPa. Fractographic investigations revealed large regions of neighbouring facets at the initiation site(s). Facets were found to be due to near-basal plane cracking and observed in grains oriented with their c-axis between 0–90° to the principal loading direction. Grains responsible for initiation were limited to orientations between 15–40°, requiring a combination of shear stress and a tensile component for cracking. Remaining orientations have been shown to accommodate faceted crack growth. The number of grains oriented for basal cracking was qualitatively related to the fatigue performance of the three product forms and found to be inversely proportional, i.e., the larger the number of unfavourably oriented grains the poorer the high cycle fatigue performance. Microtextured regions comprising of grains with their c-axis oriented within 15° from the principal loading direction have been illustrated to provide links/paths for faceted crack growth between grains favourably oriented for crack initiation.

References

[1] G. Lutjering. Influence of processing on microstructure and mechanical properties of (α+β) titanium alloys. *Materials Science and Engineering A*, 243(1-2):32–45, 1998.

[2] J. C. Williams and G. Lutjering. Effect of slip length and slip character on titanium alloys. In H. Kimura and O. Izumi, editors, *Titanium '80 : Science and Technology, Proceedings of the fourth international conference on titanium*, page 671, Kyoto, Japan, 1980. Metallurgical Society of Aime.

[3] M. Peters, A. Gysler, and G. Lutjering. Influence of texture on fatigue properties of Ti-6Al-4V. *Metallurgical and Materials Transactions A*, 15(8):1597–1605, 1984.

[4] M. R. Bache and W. J. Evans. Impact of texture on mechanical properties in an advanced titanium alloy. *Materials Science and Engineering A*, 319-321:409–414, 2001.

[5] V. Sinha, M. Mills, and J. Williams. Crystallography of fracture facets in a near-alpha titanium alloy. *Metallurgical and Materials Transactions A*, 37(6):2015–2026, 2006.

[6] C. M. Ward-Close and C. J. Beevers. The influence of grain-orientation on the mode and rate of fatigue crack-growth in alpha-titanium. *Metallurgical Transactions A - Physical Metallurgy and Materials Science*, 11(6):1007–1017, 1980.

[7] M. R. Bache, M. Cope, H. M. Davies, W. J. Evans, and G. Harrison. Dwell sensitive fatigue in a near alpha titanium alloy at ambient temperature. *International Journal of Fatigue*, 19(93):83–88, 1997.

[8] W. J. Evans and M. R. Bache. Dwell-sensitive fatigue under biaxial loads in the near-alpha titanium alloy IMI685. *International Journal of Fatigue*, 16:443–452, 1994.

[9] A. N. Stroh. The formation of cracks as a result of plastic flow. In *Proceedings of the Royal Society A-Mathematical Physical and Engineering Sciences*, volume 223, pages 404–414, 1954.

[10] F. P. E. Dunne, D. Rugg, and A. Walker. Lengthscale-dependent, elastically anisotropic, physically-based hcp crystal plasticity: Application to cold-dwell fatigue in ti alloys. *International Journal of Plasticity*, 23(6):1061–1083, 2007.

[11] D. Deka, D. S. Joseph, S. Ghosh, and M. J. Mills. Crystal plasticity modeling of deformation and creep in polycrystalline Ti-6242. *Metallurgical and Materials Transactions A-Physical Metallurgy and Materials Science*, 37A:1371–1388, 2006.

[12] G. Venkatramani, S. Ghosh, and M. Mills. A size-dependent crystal plasticity finite-element model for creep and load shedding in polycrystalline titanium alloys. *Acta Materialia*, 55:3971–3986, 2007.

[13] R. S. Bellows, S. Muju, and T. Nicholas. Validation of the step test method for generating Haigh diagrams for Ti-6Al-4V. *International Journal of Fatigue*, 21(7):687–697, 1999.

[14] D. C. Slavik, J. A. Wert, and R. P. Gangloff. Determining fracture facet crystallography using electron backscatter patterns and quantitative tilt fractography. *Journal of Materials Research*, 8(10):2482–2491, 1993.

[15] V. Hasija, S. Ghosh, M. J. Mills, and D. S. Joseph. Deformation and creep modeling in polycrystalline Ti-6Al alloys. *Acta Materialia*, 51:4533–4549, 2003.

[16] S. Ando, Y. Mine, H. Tonda, and K. Takashima. Fatigue crack growth behaviour in titanium single crystals. In G. Luetjering and J. Albrecht, editors, *Ti-2003 Science and Technology; Proceedings of the 10th world conference on titanium*, pages 1932–1940, CHH-Congress Center Hamburg, Germany, 2003. Wiley-VCH.

[17] A. W. Bowen. The influence of crystallographic orientation on fatigue crack growth in strongly textured Ti-6Al-4V. *Acta Metallurgica*, 23:1401–1409, 1975.

[18] F. Bridier, P. Villechaise, and J. Mendez. Slip and fatigue crack formation processes in an α/β titanium alloy in relation to crystallographic texture on different scales. *Acta Materialia*, 56(15):3951–3962, 2008.

[19] E. E. Sackett, L. Germain, and M. R. Bache. Crystal plasticity, fatigue crack initiation and fatigue performance of advanced titanium alloys. *International Journal of Fatigue*, 29:2015–2021, 2007.

[20] D. Rugg, M. Dixon, and F. P. E. Dunne. Effective structural unit size in titanium alloys. *Journal of Strain Analysis for Engineering Design*, 42(4):269–279, Apr 2007.

[21] V. Sinha, M. Mills, J. Williams, and J. Spowart. Observations on the faceted initiation site in the dwell-fatigue tested Ti-6242 alloy: Crystallographic orientation and size effects. *Metallurgical and Materials Transactions A*, 37(5):1507–1518, 2006.

[22] M. R. Bache, W. J. Evans, B. Suddell, and F. R. M. Herrouin. The effects of texture in titanium alloys for engineering components under fatigue. *International Journal of Fatigue*, 23(Supplement 1):153–159, 2001.

[23] W. J. Evans, J. P. Jones, and M. T. Whittaker. Texture effects under tension and torsion loading conditions in titanium alloys. *International Journal of Fatigue*, 27:1244–1250, 2005.

[24] K. Le Biavant, S. Pommier, and C. Prioul. Local texture and fatigue crack initiation in a Ti-6Al-4V titanium alloy. *Fatigue and Fracture of Engineering Materials and Structures*, 25(6):527–545, 2002.